JACS
JOURNAL OF THE AMERICAN CHEMICAL SOCIETY
Article
pubs.acs.org/JACS

Dehydration Pathways of 1-Propanol on HZSM-5 in the Presence and Absence of Water

Yuchun Zhi,[†] Hui Shi,[‡] Linyu Mu,[†] Yue Liu,[†] Donghai Mei,[‡] Donald M. Camaioni,[‡] and Johannes A. Lercher*[,†,‡]

[†]Department of Chemistry and Catalysis Research Institute, Technische Universität München, Lichtenbergstrasse 4, 85748 Garching, Germany

[‡]Institute for Integrated Catalysis, Pacific Northwest National Laboratory, P.O. Box 999, Richland, Washington 99352, United States

Supporting Information

ABSTRACT: The Brønsted acid-catalyzed gas-phase dehydration of 1-propanol (0.075−4 kPa) was studied on zeolite H-MFI (Si/Al = 26, containing minimal amounts of extra framework Al moieties) in the absence and presence of co-fed water (0−2.5 kPa) at 413−443 K. It is shown that propene can be formed from monomeric and dimeric adsorbed 1-propanol. The stronger adsorption of 1-propanol relative to water indicates that the reduced dehydration rates in the presence of water are not a consequence of the competitive adsorption between 1-propanol and water. Instead, the deleterious effect is related to the different extents of stabilization of adsorbed intermediates and the relevant elimination/substitution transition states by water. Water stabilizes the adsorbed 1-propanol monomer significantly more than the elimination transition state, leading to a higher activation barrier and a greater entropy gain for the rate-limiting step, which eventually leads to propene. In a similar manner, an excess of 1-propanol stabilizes the adsorbed state of 1-propanol more than the elimination transition state. In comparison with the monomer-mediated pathway, adsorbed dimer and the relevant transition states for propene and ether formation are similarly, while less effectively, stabilized by intrazeolite water molecules.

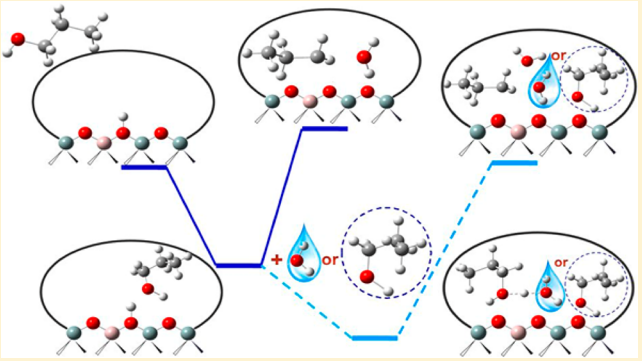

INTRODUCTION

Plant biomass represents an abundant, carbon-neutral alternative to traditional fossil resources to generate energy carriers and chemicals. Upgrading of biomass to liquid fuels requires extensive removal of multiple oxygen-containing functionalities, one of them being OH groups. Dehydration of alcohols is, therefore, a highly important class of oxygen-removal reactions involved in the catalytic transformation of biomass-derived aliphatic alcohols, polyols, as well as phenols. Relevant examples include dehydration of "bio-ethanol" to "bio-ethene",[1,2] selective dehydration of glycerol to fine chemicals,[3−5] and dehydration of cycloalkanols involved in the tandem reactions of phenols to cycloalkanes.[6]

Alcohol dehydration can be catalyzed by a variety of solid acids (the favored counterparts over liquid acids) containing either or both of Brønsted and Lewis acid sites. The site requirement for alcohol dehydration over solid acids has been subject to a number of fundamental studies; however, controversies still exist concerning whether the active sites are Brønsted or Lewis acid in nature, especially in the presence of water, a co-product of the reaction. Metal oxides are the oldest class of solid acids and bases studied for alcohol dehydration; they, however, exhibit significant surface heterogeneity, which can be affected even more by pretreatment/reaction conditions (temperature, adventitious impurities/water, etc.), causing contradictory mechanistic conclusions.[7,8] Compared to metal oxides with diverse surface and acid properties, zeolites have relatively well-defined and uniform Brønsted acid site (BAS) structures, which lend themselves to rigorous kinetic and theoretical investigations on the requirement of acid strength, the effect of solvation environment, and reaction mechanisms for alcohol dehydration.

The medium pore zeolite HZSM-5, of MFI-type framework, plays a preeminent role in a multitude of petrochemical processes, including isomerization of xylene,[9,10] methanol-to-hydrocarbons (MTG/O/P),[11−16] alkylation, and disproportionation of aromatics.[9,17−19] HZSM-5 is also known to be active in gas phase and liquid phase dehydration of monoalcohols[20−25] and polyols.[26,27] Zamaraev, Thomas, and co-workers are pioneers in probing the effect of pore confinement in the dehydration of butanol isomers over MFI samples.[20,23−25] In one of these seminal works,[23] they observed a direct correlation of isobutanol dehydration rates with the concentration of BAS, while no correlation was found with Lewis acid site (LAS) concentration. *In situ* titration experiments using hindered

Received: August 27, 2015
Published: November 11, 2015

DOI: 10.1021/jacs.5b09107
J. Am. Chem. Soc. 2015, 137, 15781−15794

pyridines demonstrate that LAS do not contribute detectably to methanol dehydration rates over MFI zeolites.[28] Gorte et al.[29−31] reported that the concentration of strongly adsorbed C1−C4 alcohol molecules on MFI samples corresponds to the Al^{3+} concentration in the zeolite lattice, i.e., Brønsted-acidic sites, irrespective of the Si/Al ratio.

Recently, kinetics and mechanism of dehydration of methanol and ethanol were thoughtfully investigated over zeolites, including H-MFI.[21,22] In both studies, only ether formation was identified, because methanol does not form a stable gaseous olefin product, whereas ethanol dehydration to ethene was kinetically unfavorable over H-MFI at the applied temperatures (368−409 K). In addition, Kondo et al. systematically investigated by infrared spectroscopy the mechanism and activation energies of the decomposition of surface ethoxy species to ethene, a possible elementary step in ethanol dehydration over zeolites.[32,33] However, neither the crucial step of ethanol dehydration to form ethoxy intermediate nor the ether formation pathway was involved and discussed. Thus, a complete and rigorous kinetic and mechanistic assessment on both intra- and intermolecular pathways of alcohol dehydration is still lacking for MFI zeolites and, similarly so, for other solid acids.

Another significant concern that prompts us to revisit alcohol dehydration relates to the fact that real biomass feedstocks contain large quantities of water. Kinetic inhibition of water has been frequently reported for alcohol dehydration on solid acids.[34,35] In the context of zeolites, water can influence the kinetics of alcohol dehydration, potentially by competing with alcohol reactants for BAS, by shifting the dehydration/hydration equilibrium, and by inducing potentially different solvation strengths to all states along the reaction coordinate in zeolite confines. In addition, water may modify the nature of the active sites,[36] where a framework proton may not be able to adequately describe the real Brønsted acid site structure during steady-state catalysis in the presence of water. Water adsorption at the zeolitic proton site has been proposed to result in formation of a neutral hydrogen-bonded (H-bonded) complex and/or an ion-pair complex.[37−45] It remains debatable as to whether the two complexes are both local minima on the potential energy surface separated by an energy barrier, or one of the two is actually a saddle point of first order (i.e., a transition state).[44] A zeolitic proton will become attenuated in acid strength, if it is transferred to two or more water molecules, forming protonated water clusters (hydronium ions).

In this contribution, we explore the enthalpic and entropic factors that govern the kinetics of 1-propanol dehydration via mono- and bimolecular routes catalyzed within the host environments of an extraframework Al-free H-MFI at 413−443 K. Mechanisms for propene and dipropyl ether (DPE) formation have been developed, which are used to interpret the kinetic effects of temperature and 1-propanol/water pressures over a wide range of surface coverages. The finding that adsorbed alcohol monomer and dimer are both reactive intermediates for propene formation in H-MFI contrasts previous conclusions on the unreactive nature of the dimer species for alcohol dehydration catalysis over POM clusters and acidic zeolites.[21,34,35] The nature of the interaction of 1-propanol and water with H-MFI is probed by *in situ* IR spectroscopy as well as gravimetric and calorimetric methods; we show unequivocally that kinetic inhibition of dehydration by water is not a consequence of competitive adsorption between 1-propanol and water. By combining in-depth kinetic assessments and density functional theory (DFT) simulations, we quantify reaction pathways explaining unequivocally the roles of co-fed water as well as of increasing concentrations of 1-propanol.

RESULTS AND DISCUSSION

Catalyst Characterization. To minimize the effects of extra-framework Al (EFAL) on the acidity and local environment of BAS, $(NH_4)_2SiF_6$ (denoted as AHFS) was used to preferentially remove the EFAL from the parent MFI-15 sample (see Experimental and Theory Section). The physicochemical properties of parent and AHFS-treated MFI samples, in their proton-forms, are presented in Table 1.

Table 1. Physicochemical Properties of Parent H-MFI-15 and AHFS-Treated H-MFI-15

samples	Si:Al[a]	S_{BET}[b] $m^2\ g^{-1}$	V_{micro}[b] $cm^3\ g^{-1}$	BAS[c] $\mu mol\ g^{-1}$	LAS[c] $\mu mol\ g^{-1}$
H-MFI-15	15	423	0.164	837	211
H-MFI-15-AHFS	26	427	0.159	693	55

[a]Molar ratio of Si and Al determined by AAS. [b]Micropore volume determined by N_2 adsorption. [c]Acid concentrations determined by IR spectroscopy of adsorbed pyridine.

Specific surface areas and micropore volumes of the parent and the AHFS-treated MFI zeolites are very similar, confirming the nondestructive character of the AHFS treatment. SEM micrographs of the parent and AHFS-treated samples indicate that the diameter of primary crystallites is smaller than 1 μm for both cases (not shown). After AHFS modification, the Si/Al ratio increased from 15 to 26, indicating removal of Al from the zeolite structure. Concurrently, the concentration of BAS decreased from 837 to 693 $\mu mol\ g^{-1}$, whereas the LAS concentration decreased by approximately 75% from 211 to 55 $\mu mol\ g^{-1}$, demonstrating that significant concentrations of EFAL species were removed by the treatment. The removal of EFAL debris was also confirmed by the IR spectra of hydroxyl stretching vibration of AHFS-treated H-MFI-15 sample (Figure 1).

Both samples exhibit the characteristic bands at 3610 and 3745 cm^{-1}, corresponding to a bridging hydroxyl group acting as a BAS and a surface terminal silanol group, respectively.[46,47] Two additional bands at 3665 and 3780 cm^{-1} for the parent zeolite are attributed to OH bands of octahedral EFAL moieties such as charged or neutral aluminum oxides and aluminum hydroxides.[46,48] The bands disappeared after AHFS treatment, suggesting that EFAL species have been essentially removed. The removal of EFAL allows us to specifically assess the mechanism and kinetics of the alcohol dehydration reaction taking place on BAS in the absence of synergistic effects exerted by LAS.[46,48,49] All subsequent characterizations and catalytic measurements were performed on the AHFS-treated H-MFI catalyst.

The coverage dependences for the differential heats of adsorption of 1-propanol in the pressure range from 10^{-4} to 1.2 kPa at 323 K are presented in Figure 2. The corresponding adsorption isotherm is presented in Figure 1S (Supporting Information). For the first exposure of zeolite sample to 1-propanol vapor under an equilibrium pressure of 10^{-4} kPa, the initial heats of adsorption were around −120 kJ mol^{-1}

DOI: 10.1021/jacs.5b09107
J. Am. Chem. Soc. 2015, 137, 15781−15794

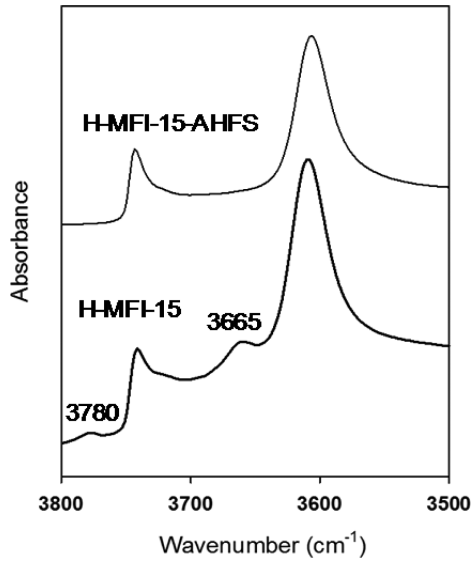

Figure 1. Infrared spectra of hydroxyl stretching vibration region of activated parent and AHFS-treated H-MFI-15 samples.

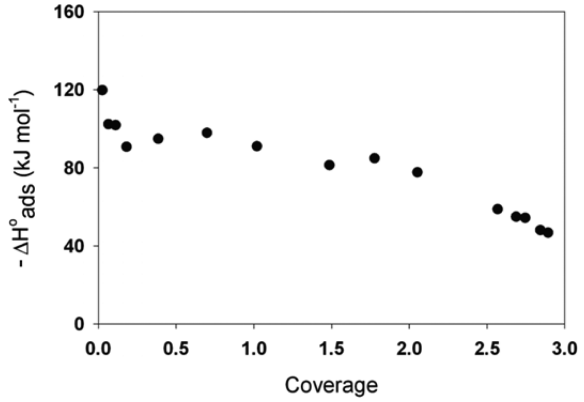

Figure 2. Differential heats of adsorption as a function of 1-propanol coverage for H-MFI-15-AHFS sample at 323 K.

associated with a coverage of 0.025. Thamm[50] and Gorte et al.[51] observed similar or somewhat higher heats of adsorption for C1−C4 alcohols on HZSM-5 at very low coverages. The authors attributed the high initial heat of adsorption to the interaction of 1-propanol with defect sites of the sample.[50,51] The catalyst used in the present work has been subjected to AHFS treatment and, thus, could be considered as a "clean" sample. More likely in our case, the initial heats of adsorption do correspond to the interaction strength of 1-propanol with the Brønsted acidic framework sites. The heat of adsorption was roughly constant at a value of -92 ± 9 kJ mol^{-1} for coverages from 0.065 to 2.0. This suggests that 1-propanol adsorption continues to be localized at acid sites and the appearance of adsorbate/adsorbate interactions associated with the acid sites that correspond to formation of 1-propanol dimer over one BAS.[51] As we analyze later, the surface concentration of the 1-propanol dimer already starts to dominate over that of the monomer species at uptakes as low as 0.15 molecule/site at 323 K (i.e., where calorimetric and isotherm measurements were conducted). At this moment, however, the relative contributions of the adsorbed 1-propanol monomer and dimer species to the measured heats of adsorption cannot be derived from calorimetry and adsorption isotherm measurements without knowing adsorption equilibrium constants for both species. The individual adsorption enthalpies for the monomer and dimer species on BAS will be derived later. The decrease in the heat of adsorption beyond a coverage of two molecules/site is related to the contribution of adsorption at the external surface of the zeolite particles, which is close to the heat of condensation for 1-propanol (∼−45 kJ mol^{-1}).

Kinetics and Mechanism of 1-Propanol Elimination to Propene. The gas-phase dehydration of 1-propanol was studied in a wide range of partial pressure of 1-propanol (0.075−4 kPa) at 413−443 K, in the absence and presence of co-fed water. Propene and DPE were observed as the parallel products from unimolecular and bimolecular dehydration reactions. In this section, we analyze the unimolecular dehydration pathway that produces propene. The regressed kinetic and thermodynamic parameters for the quasi-equilibrated adsorption and protonation steps as well as the rate-limiting elimination step, based on a rate equation derived from the proposed pathway (Scheme 1), were used to interpret the observed effects of 1-propanol/water pressure and temperature on reaction rates.

Effects of 1-Propanol Pressure and Temperature on Turnover Rates. Turnover rates reported in this work were determined by normalization of the mass-specific rates (measured at steady state) by the concentration of BAS (Table 1). Importantly, no deactivation was detected during kinetic measurements. It is imperative that rates be measured at conversions lower than 1% or, more preferably, obtained by extrapolation to zero residence time, as a result of the dampening effects of water that is formed during reaction (to be discussed in the following sections). For instance, rates decreased already by ca. 10% at conversions as low as 2% at 423 K (Figure 2S). Therefore, the rates reported in this work were all measured at conversions lower than 1.5%. The measured turnover rates for propene formation are shown in Figure 3 as a function of 1-propanol pressure (0.075−4 kPa) on the EFAL-free H-MFI. Propene formation rates decreased with increasing 1-propanol pressure and then gradually leveled off, both in the absence and presence of co-fed water (Figures 3 and 3S). The observed negative effects of the alcohol pressure on the intramolecular dehydration rate are in qualitative agreement with previous reports on ethanol dehydration over H-MOR zeolites[21] and $H_3PW_{12}O_{40}$,[52] as well as 2-butanol dehydration and *sec*-butyl-methyl ether cleavage over a variety of polyoxometalate (POM) clusters.[34,53] The decrease in reaction rates with increasing pressure of the alcohol was commonly ascribed to the formation of (protonated) unreactive alcohol dimers occupying acid sites, thus inhibiting the overall dehydration reaction. The stable and unreactive nature of 2-butanol dimers was inferred from estimates using DFT indicating that 2-butanol dimer is 84 kJ mol^{-1} enthalpically more stable than the 2-butanol monomer.[54] Propene formation rates also decreased as water vapor was co-fed (Figures 3b and 3S). However, removing water vapor from the 1-propanol feed completely restored the activities, indicating no permanent change of the active site. Prior to discussing the origins of the observed pressure dependences of, and the inhibition effect of water on, propene formation rates, we will propose, and validate using DFT calculations, the elementary steps for the monomolecular dehydration.

Elementary Steps for 1-Propanol Conversion to Propene. A proposed sequence of elementary steps (or lumped steps) for 1-propanol dehydration to propene is

DOI: 10.1021/jacs.5b09107
J. Am. Chem. Soc. 2015, 137, 15781−15794

Scheme 1. A Proposed Sequence of Elementary Steps for 1-Propanol Elimination to Form Propene over a Zeolitic Proton

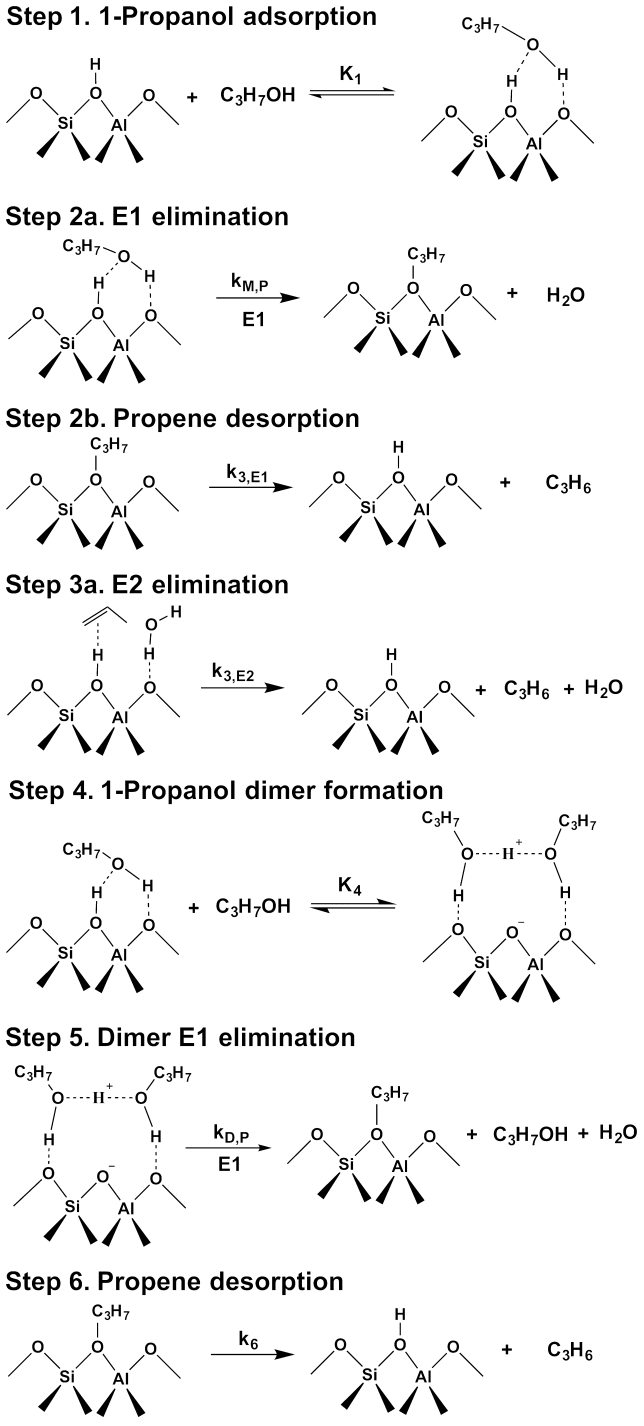

presented in Scheme 1. Diffusion of reactant and products into and out of the pores is not depicted. The catalytic cycle is initiated by the quasi-equilibrated adsorption of 1-propanol on BAS to form the H-bonded 1-propanol monomer (Step 1, Scheme 1). The 1-propanol monomer can also interact with another 1-propanol (in the pore) to form a protonated dimer (Step 4). In this work, routes via 1-propanol monomer and dimer are shown to exist. In the monomer route, the H-bonded 1-propanol is protonated and transformed to an alkoxonium ion, which is H-bonded to two zeolite O atoms adjacent to the Al atom. Although we have omitted this protonation step in Scheme 1, it seems to be essential for the subsequent cleavage of C−O bond, as suggested by DFT calculations shown next (see Supporting Information for detailed considerations).

Elimination of the protonated 1-propanol species occurs via either an E1-like (stepwise) or an E2-like (concerted) mechanism.[34,53,55] Even though long-standing controversies exist on the prevalence of an E1 or E2 sequence in water elimination from an alcohol,[7,56,57] reasonable agreement based on experiments[21,58] and theoretical calculations[34,54] suggests that lower alcohols tend to eliminate water via an "E1" mechanism on acidic zeolites or POM clusters. There are multiple possible paths that can be seen as E1-like or have more E1 character; a probable path that produces 1-propoxide is depicted as Step 2a in Scheme 1. Strictly speaking, this particular step should be seen as a nucleophilic substitution, rather than a true elimination reaction. Yet, a similar nomenclature was used for describing elimination of alcohol which forms surface alkoxide on solid acids.[21,34] Regardless, the nature of the resting state following the C−O cleavage, be it surface alkoxide, carbenium ion, or physisorbed alkene, would not matter to the kinetic derivations. As the final step, deprotonation of the adsorbed 1-propoxide generates propene (Step 2b, Scheme 1). Alternatively, the E2-like pathway involves concerted cleavage of C_α−O and C_β−H bonds in the 1-propanol monomer, most likely after reorientation of its configuration, forming physisorbed propene and water concurrent with proton transfer back to the zeolite (Step 3a). Desorption regenerates the active site (Step 3b).

E1- and E2-types of dehydration mechanisms yield equivalent rate formalisms and, thus, cannot be discriminated from the kinetic data shown in Figure 3. For the scenarios of the present case, the potential E1 and E2 pathways for dehydration were explored by DFT calculations. The energies and optimized configuration of intermediates and transition states for 1-propanol adsorption and dehydration on a periodic H-MFI model for both E1-like and E2-like routes are shown in Figures 4 and 4S, respectively. Both pathways share the adsorption of 1-propanol at a BAS via H-bonding (A in Figure 4). The calculated 1-propanol adsorption energy is −105 kJ mol^{-1} with van der Waals (vdW) and zero-point energy (ZPE) corrections, which is a little lower than the derived heat of adsorption of −120 kJ mol^{-1} (discussed later). Upon adsorption, the protonation of 1-propanol by the zeolite proton (H_z) is facile with a low barrier of 6 kJ mol^{-1}, indicative of the quasi-equilibrium between H-bonded and protonated 1-propanol adsorption states (B in Figure 4). Additionally, the enthalpic difference between these two adsorption intermediates was just 5 kJ mol^{-1}, which concurs with a similar observation for methanol interaction with the BAS of zeolites.[59] The difference in free energy is somewhat greater, with the protonated alcohol state being 16 kJ mol^{-1} less stable (Figure 5S). We further performed an ab initio molecular dynamics (AIMD) simulation of the protonation of 1-propanol at 500 K and observed quick and facile proton transfer to 1-propanol. Using slow annealing of the AIMD simulated configuration as well as the frequency analysis, the formed oxonium complex of $[CH_3CH_2CH_2OHH_z]^+$ (B in Figure 4, H_z being the zeolitic proton) was further substantiated as a reactive intermediate state, rather than a transition state. This is also consistent with the previous calculations of 1-propanol in HZSM-5,[60,61] but is at variance with adsorption structures suggested for methanol.[44,59] Upon protonation, the C_α−O bond in the adsorbed

DOI: 10.1021/jacs.5b09107
J. Am. Chem. Soc. 2015, 137, 15781−15794

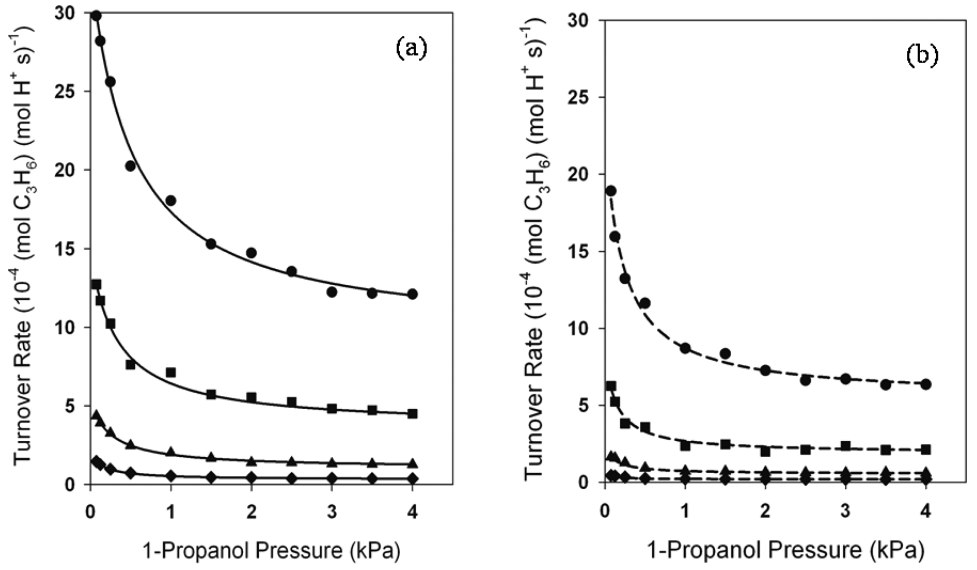

Figure 3. Measured propene turnover rates (per H^+) as a function of 1-propanol pressure (0.075−4 kPa) over H-MFI-15-AHFS at 413 K (◆), 423 K (▲), 433 K (■), and 443 K (●). The solid and dash curves represent the fitting of experimental data points to eq 4: (a) in the absence of co-fed water and (b) in the presence of co-fed water (P_{water} = 0.53 kPa).

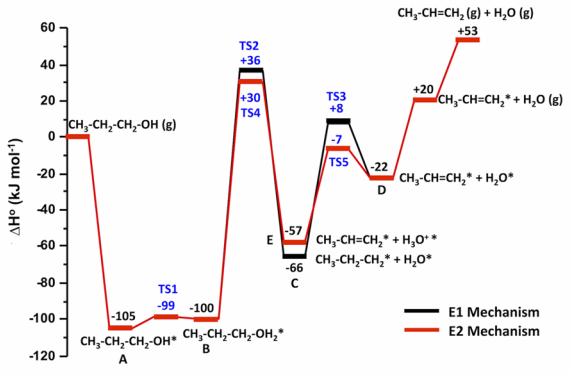

Figure 4. DFT-calculated energy diagram for 1-propanol dehydration over H-MFI via the monomer-mediated route: E1-like (black line) and E2-like mechanisms (red line). All values are at 433 K.

1-propanol elongates from 147 to 156 pm, indicating a weakening of the C_α−O_{alc} bond strength which in turn facilitates the following elimination/substitution reactions that cleave the C_α−O_{alc} bond.

In the rate-limiting step via an E1-like mechanism, the protonated 1-propanol is dissociated into water and the propoxide intermediate (C in Figure 4). This step is endothermic (+34 kJ mol^{-1}) with an activation barrier of 136 kJ mol^{-1}. The transition state (TS2 in Figure 4) for the E1-like elimination route is characterized by a carbenium-ion-like structure, as indicated by sp^2 hybridization in which the substituents of the C_α atom are in the same plane.[54] In this transition-state geometry, the length of the C_α−O_{alc} bond is 248 pm, almost completely broken. Additionally, the Mulliken charge for the $[C_3H_7]$ fragment and the water molecule were found to be +0.70 |e| and +0.05 |e|, respectively. Altogether, the charge distribution, energy, and configuration of TS2 resemble those of the elimination product, suggesting that the E1-like pathway has a late transition state. Note that although a carbenium-ion-like transition state is observed, formation of a stable carbocation intermediate characteristic of a pure, classical E1 mechanism has never been captured by our DFT calculations. The following deprotonation of the propoxide to form adsorbed propene (D in Figure 4) is also endothermic (+44 kJ mol^{-1}), and the activation barrier is 74 kJ mol^{-1}, which is significantly lower compared to the barrier for water elimination (136 kJ mol^{-1}). Consequently, the C_α−O_{alc} bond cleavage in the E1-like pathway is the kinetically relevant step, a conclusion in agreement with the solid acid-catalyzed elimination for ethanol[21,62] and 2-butanol.[34,54]

Following the E2-like mechanism, the protonated 1-propanol (B in Figure 4) decomposes concertedly to propene and the hydronium (H_3O^+) (E in Figure 4) with an activation barrier of 130 kJ mol^{-1}. The hydronium (H_3O^+) transfers the proton back to the zeolite forming water, which then desorbs.

Since the protonated alcohol state is less populated than the H-bonded state due to a higher free energy (−41 vs −57 kJ mol^{-1}; Figure 5S), the measured activation energy corresponds to the energy difference between the elimination transition state and the H-bonded state. The DFT-derived enthalpic differences of transition state (TS2 and TS4 in Figure 4) relative to the H-bonded state (A in Figure 4) are 141 and 135 kJ mol^{-1} for E1- and E2-type mechanisms, respectively; both DFT estimates are comparable with the measured activation barrier of 142 kJ mol^{-1} (details shown later). The similar calculated activation energies for E1- and E2-like mechanisms suggest that the prevalence of E1- or E2-like type elimination cannot be enthalpically differentiated. To discern which type of mechanism is more likely, the entropic contributions in the rate-determining step were calculated using eq 1:

$$k = \frac{k_B T}{h}\exp\left(\frac{\Delta S^{\ddagger}}{R}\right)\exp\left(\frac{-\Delta H^{\ddagger}}{RT}\right) = A\ \exp\left(\frac{-\Delta H^{\ddagger}}{RT}\right) \quad (1)$$

The calculated activation entropies with respect to the elimination step for E1- and E2-like mechanisms were 28 and 3 J mol^{-1} K^{-1}, respectively, resulting in 1 order of magnitude larger pre-exponential factor for the E1-like route (2.6×10^{14} s^{-1}) than the E2-like route (1.3×10^{13} s^{-1}). Taking into account both calculated enthalpies and entropies, the ratio of rate constants for the E1-like path and the E2-like path would

DOI: 10.1021/jacs.5b09107
J. Am. Chem. Soc. 2015, 137, 15781−15794

be around 2.9, implying that the E1-like mechanism is slightly favored. The higher activation entropy for the E1-like pathway compared to the E2-like pathway is associated with the simultaneous C_α−O bond activation and C_β−H interaction with the zeolite oxygen leading to a more ordered structure, which results in a substantial loss of entropy relative to chemisorbed intermediate.[34]

In the following, the rate expression for water elimination from 1-propanol at low conversions is derived assuming quasi-equilibrated 1-propanol adsorption, irreversible water elimination, and propene desorption and acid sites to be predominantly occupied by the 1-propanol monomer and protonated dimer. The inclusion of vacant site coverage is not supported by the spectroscopic measurements as we show later, nor does it yield good fitting results.

If the dimer species is unreactive in mediating the intramolecular dehydration, as concluded for 2-butanol dehydration over POM clusters,[34] one arrives at the following rate equation, by combining the elementary steps depicted in Scheme 1 (Steps 1−4) with the foregoing analysis that the kinetically relevant step is the C−O bond cleavage (derivations given in the Supporting Information):

$$\frac{r_{C_3H_6}}{[H^+]_0} = \frac{k_{M,P}}{(1 + K_4[C_3H_7OH])} \quad (2)$$

where $k_{M,P}$ and K_4 are the rate constant for water elimination from monomeric 1-propanol (step 2, Scheme 1) and the equilibrium constant for 1-propanol dimer formation (step 4, Scheme 1), respectively, while $[H^+]_0$ is the initial concentration of the accessible BAS. Eq 2 can be rewritten into a linear form, eq 3:

$$\frac{[H^+]_0}{r_{C_3H_6}} = \frac{1}{k_{M,P}} + \frac{K_4[C_3H_7OH]}{k_{M,P}} \quad (3)$$

It is expected from eq 3 that the linear dependence of inverse propene formation rate on 1-propanol pressure would give rise to accurate estimates of $k_{M,P}$ and K_4. However, the inverse turnover rate of propene formation increases monotonically but nonlinearly, and the regression of experimental data to eq 3 is inconsistent with the measured variations of the inverse rate as the 1-propanol pressure changes (Figure 5). This implies that 1-propanol monomer cannot be the only reactive intermediate for propene formation and that the protonated 1-propanol dimer must also decompose to generate propene under high-pressure conditions. This is the first instance where dimeric alcohol species is demonstrated to be reactive in mediating intramolecular alcohol dehydration over solid acids, in stark contrast to results of ethanol dehydration over H-MOR at 368−409 K[21] and 2-butanol dehydration over POM clusters at 333−373 K.[34] It is noteworthy that the current results were obtained in a significantly wider window of alcohol partial pressure (0−4 kPa) than that in the Iglesia et al. work (0−0.5 kPa).

On this basis, we propose that the dimer-mediated route proceeds via the following steps to produce propene. The protonated 1-propanol dimer dissociates to form a propoxide along with water and 1-propanol (Step 5, Scheme 1). In the next step the propoxide intermediate deprotonates to form propene (Step 6, Scheme 1). Correspondingly, a revised rate equation for propene formation is developed in terms of rate contribution from both 1-propanol monomer and dimer, which

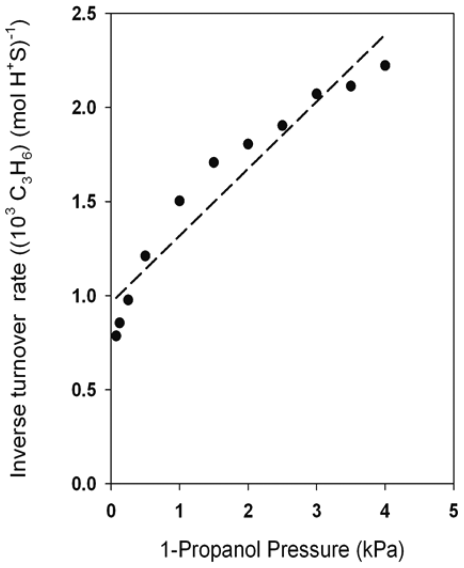

Figure 5. Inverse propene formation turnover rates as a function of 1-propanol pressure over MFI-15-AHFS at 433 K without co-feeding water. The dashed line represents regression of experimental data points to eq 3, which is derived by assuming dimer species to be unreactive while occupying a significant number of active sites.

is shown as follows (the derivation is given in the Supporting Information):

$$\frac{r_{C_3H_6}}{[H^+]_0} = \frac{k_{M,P} + k_{D,P}K_4[C_3H_7OH]}{1 + K_4[C_3H_7OH]} \quad (4)$$

where $k_{D,P}$ is the rate constant for water elimination from 1-propanol dimer (Step 5, Scheme 1).

This revised rate equation is consistent with the observation that propene formation rates do not decline further, but rather maintain at a relatively constant level, with increasing 1-propanol pressures (Figure 3). Therefore, the proposed mechanistic sequence for propene formation (Scheme 1) is capable of describing the experimental data accurately over a sufficiently wide range of conditions (413−443 K, 0.075−4 kPa 1-propanol, 0−2.5 kPa H_2O). By deconvolution of turnover rates for propene formation, the respective contribution of 1-propanol monomer and dimer intermediates to form propene is presented in Figure 6, taking the measured rates at 433 K as an example. With the increase in reactant pressure, the rate of propene formation gradually decreases in parallel with the progressive increase in the dimer-mediated route.

Kinetic and Thermodynamic Constants for Propene Formation via Monomer- and Dimer-Mediated Routes in the Absence and Presence of Co-Fed Water. The rate constants $k_{M,P}$, $k_{D,P}$ (for the corresponding rate-determining step in monomer- and dimer-mediated propene formation routes) as well as the equilibrium constant, K_4, for 1-propanol dimer formation are determined from regression of the measured propene formation rates at four different temperatures (Figure 3a) into eq 4 in the absence of co-fed water. The results are tabulated in Table 2. The two kinetically relevant rate constants, $k_{M,P}$ and $k_{D,P}$, reflect the changes in the standard free energy from the adsorbed 1-propanol monomer and dimer species to their respective elimination transition state. The rate constant for the C−O bond cleavage in the 1-propanol monomer ($k_{M,P}$) is larger than the corresponding rate constant for the 1-propanol dimer ($k_{D,P}$) at each specific temperature,

DOI: 10.1021/jacs.5b09107
J. Am. Chem. Soc. 2015, 137, 15781−15794

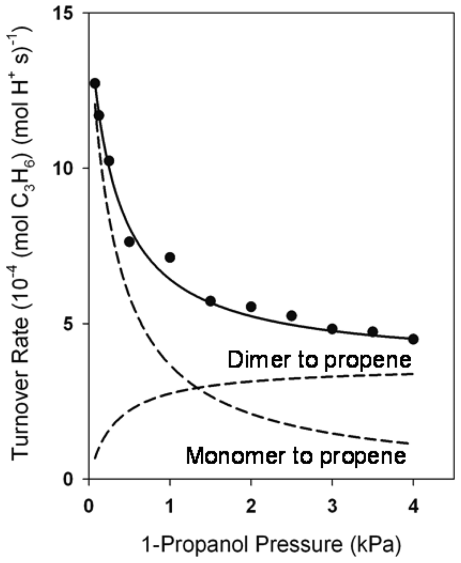

Figure 6. Deconvolution of turnover rate for propene formation to the respective contributions from monomer- and dimer-mediated routes in 1-propanol dehydration reaction over H-MFI-15-AHFS at 433 K in the absence of co-fed water.

Table 2. 1-Propanol Monomer to Propene Rate Constant $k_{M,P}$, 1-Propanol Dimer to Propene Rate Constant $k_{D,P}$, and 1-Propanol Dimer Formation Equilibrium Constant K_4 (see Scheme 1) for 1-Propanol Dehydration Over H-MFI-15-AHFS in the Absence of Co-Fed Water[a]

T (K)	$k_{M,P}$ 10^{-4} (H^+ s)$^{-1}$	$k_{D,P}$ 10^{-4} (H^+ s)$^{-1}$	K_4 (kPa^{-1})
413	2.1	0.3	6.7
423	5.4	1.0	4.2
433	14.8	3.7	2.9
443	33.0	9.3	2.0

[a]Parameters are determined by fitting eq 4 to experimental data (Figure 3a).

reflecting the relatively lower reactivity of the latter. From the values of K_4, the coverage of the 1-propanol dimer must be significant in the whole range of the applied reaction conditions. The monomer coverage becomes small (<0.1) at low temperatures and high 1-propanol pressures and even more so when water is present.

The K_4 value for 1-propanol dimer formation, extrapolated to 368 K, is much lower (73 vs 1859 kPa^{-1}) than that reported by Chiang and Bhan[21] for ethanol dimer formation on HZSM-5 (Si/Al = 42.6) at the same temperature. This dramatic difference is in large part due to the difference in size of the monomers and dimers in comparison to the pore size of HZSM-5 zeolite. We surmise that confinement in the pore limits the larger propanol molecules from attaining their most stable configurations on the active site. Steric constraints in the pore also limit the degrees of freedom of adsorbed propanol to greater degree than adsorbed ethanol. Thus, the entropy of forming the propanol dimer should be less than that of forming the ethanol dimer. As a result, the equilibrium constant for dimer formation is much less favorable in the case of 1-propanol than ethanol.

Water can impact the unimolecular dehydration by affecting the surface coverage of reactive intermediates and/or the solvation environments of resting states and transition states. An irreversible structural change in the nature/structure of acid sites is impossible here, in view of the fully restorable activity upon removing co-fed water (*vide infra*).

A full coverage of surface acid sites was achieved at equilibrium 1-propanol pressures above 0.04 kPa at 433 K, as evidenced by the complete disappearance of the bridging hydroxyl vibration at 3610 cm^{-1} (Figure 6S). Thus, surface acid sites are fully covered by 1-propanol species (monomer and dimer) under our actual dehydration conditions (0.075−4 kPa; 413−443 K). Moreover, IR spectra of co-adsorbed 1-propanol and water (see below) show that water is unable to remain directly associated with the BAS of zeolite in the presence of 1-propanol at similar partial pressures. A number of water molecules are, however, able to remain in the pores and interact with the adsorbed alcohol (detailed discussions presented later). This allows us to conclude that at our operating conditions, water cannot directly occupy BAS to form monomeric or dimeric water surface species, yet that it interacts laterally with adsorbed 1-propanol stabilizing the adsorption intermediates. Ison and Gorte reached similar conclusions with methanol and water, by employing deuterium exchange experiments; they showed that water is not blocked by adsorbed methanol from approaching the proton sites, though it could not displace methanol.[36]

Thus, the coverages of 1-propanol derived intermediates are unaffected by co-fed water (at least up to 2.5 kPa), and eq 4 is also applicable to the case where water is present. The kinetic and equilibrium parameters in eq 4, obtained from fitting of the experimental data in the presence of co-fed water (Figure 3b), are shown in Table 3. The rate constants of the elimination of

Table 3. Estimated 1-Propanol Monomer to Propene Rate Constant $k_{M,P}$, 1-Propanol Dimer to Propene Rate Constant $k_{D,P}$, and 1-Propanol Dimer Formation Equilibrium Constant K_4 (see Scheme 1) for 1-Propanol Dehydration over H-MFI-15-AHFS in the Presence of Co-Fed Water (0.53−2.5 kPa)[a]

T (K)	$k_{M,P}$ 10^{-4} (H^+ s)$^{-1}$	$k_{D,P}$ 10^{-4} (H^+ s)$^{-1}$	K_4 (kPa^{-1})
413	0.8	0.2	19.4
423	2.5	0.6	11.0
433	8.6	1.9	7.1
443	22.6	5.5	4.3

[a]Parameters are determined by regression of experimental data (Figure 3b) into eq 4.

water from both the 1-propanol monomer ($k_{M,P}$) and the 1-propanol dimer ($k_{D,P}$) are attenuated by the presence of water, whereas the equilibrium constant for dimer formation increases (cf. Tables 2 and 3).

Using transition state theory, the activation enthalpies and entropies for the rate-limiting C−O bond cleavage, as well as the enthalpy change associated with 1-propanol dimer formation from an adsorbed monomer and a gaseous molecule, were obtained by plotting the natural logarithm of regressed rate constants ($k_{M,P}$ and $k_{D,P}$) or equilibrium constant (K_4) against the reciprocal temperature, in the absence and presence of water (413−443 K, Figure 7S). These parameters are summarized in Table 4. The enthalpic barrier for 1-propanol dimer to propene ($\Delta H^{\ddagger}_{D,P}$ = 175 kJ mol^{-1}) is higher than for the 1-propanol monomer to propene ($\Delta H^{\ddagger}_{M,P}$ = 142 kJ mol^{-1}). Concomitantly, the activation entropies increase from 25 J mol^{-1} K^{-1} for $\Delta S^{\ddagger}_{M,P}$ to 91 J mol^{-1} K^{-1} for $\Delta S^{\ddagger}_{D,P}$.

DOI: 10.1021/jacs.5b09107
J. Am. Chem. Soc. 2015, 137, 15781−15794

Table 4. Activation Enthalpies and Entropies for 1-Propanol Elimination to Propene and Adsorption Enthalpies and Entropies for 1-Propanol Dimer Formation Over H-MFI-15-AHFS in the Absence and Presence of Co-Fed Water (0.53−2.5 kPa) at 433 K[a]

	without water	with water
$\Delta H^{\ddagger}_{M,P}$ (kJ mol^{-1})	142 ± 2	170 ± 2
$\Delta H^{\ddagger}_{D,P}$ (kJ mol^{-1})	175 ± 3	173 ± 4
$\Delta S^{\ddagger}_{M,P}$ (J mol^{-1} K^{-1})	25 ± 3	87 ± 3
$\Delta S^{\ddagger}_{D,P}$ (J mol^{-1} K^{-1})	91 ± 4	80 ± 4
ΔH^{o}_{4} (kJ mol^{-1})	−64 ± 1	−75 ± 2
ΔS^{o}_{4} (J mol^{-1} K^{-1})	−100 ± 3	−119 ± 5

[a]For calculations of activation entropies from measured rate/equilibrium constants on the basis of transition-state theory, the standard states are defined as follows: P^{o} = 100 kPa for gaseous molecules and θ = 1 for surface species.

It is interesting to compare the influence of water on the activation barriers and the dimer formation enthalpy. As shown in Table 4, the activation enthalpy of $\Delta H^{\ddagger}_{M,P}$ increases from 142 to 170 kJ mol^{-1} in the presence of water, a value comparable with the $\Delta H^{\ddagger}_{D,P}$ of 175 kJ mol^{-1}, indicating that the presence of water and of an additional 1-propanol stabilizes the ground state of adsorbed 1-propanol similarly and induces in this way a similar inhibiting effect on unimolecular dehydration. The activation entropy of $\Delta S^{\ddagger}_{M,P}$ (87 J mol^{-1} K^{-1}) in the presence of water also resembles the activation entropy in the presence of an additional 1-propanol molecule, i.e., $\Delta S^{\ddagger}_{D,P}$ (91 J mol^{-1} K^{-1}).

For the dimer formation (Step 4, Scheme 1), the associated enthalpy change (from fitting) is −64 kJ mol^{-1} without co-fed water. Different from the remarkable stabilization of the monomer by water (−82 kJ mol^{-1}, as we show later), the presence of water only induces a small stabilization effect (−11 kJ mol^{-1}) on the dimer, suggesting that the 1-propanol dimer and water do not form a mixed protonated trimer or larger structure. The concomitant entropy loss (−19 J mol^{-1} K^{-1}) does not overcompensate for the enthalpic stabilization at the prevalent conditions used here, resulting in greater dimer formation constants in the presence of intrazeolite water.

All the tabulated values in Tables 2−4 can be used, by extrapolation, to predict the prevalence of monomer- and dimer-mediated routes at other reaction conditions, as long as no new pathways open up or no new species form. The results are shown in Figure 8S. The ratio of the dimer-mediated route to the monomer-mediated one decreases with increasing temperature or decreasing 1-propanol pressures. The presence of water always enhances the dimer route over the monomer at temperatures below 463 K, while it disfavors the dimer route over the monomer route at T > 463 K, independent of the 1-propanol pressure.

Kinetics and Mechanism of 1-Propanol Dehydration to DPE. The measured turnover rates (per H^{+}) for DPE formation are shown in Figure 7 as a function of 1-propanol pressure (0.075−4 kPa) on H-MFI-15-AHFS. The turnover rates increase with increasing 1-propanol pressure and then gradually become insensitive to the 1-propanol pressure (Figure 7a). As is the case of propene formation, turnover rates for DPE formation became also lower when water was added (Figures 7b and 3S).

Two mechanisms, namely the dimer-mediated direct route and the alkoxide-mediated sequential pathway are proposed for the bimolecular alcohol dehydration over solid acids.[21,22,28,63] The direct mechanism includes the adsorption of 1-propanol to form a 1-propanol monomer (Step 1, Scheme 2) and then the co-adsorption of a second 1-propanol molecule to form protonated 1-propanol dimer (Step 2, Scheme 2). These two steps are identical to Steps 1 and 4 in Scheme 1. The dimer then decomposes to form DPE and water (Step 3, Scheme 2). In the sequential dehydration route, the adsorbed 1-propanol monomer first eliminates water to form surface-bound propoxide species (see the E1-like mechanism for propene formation in Scheme 1), followed by the reaction of the propoxide intermediate with a 1-propanol molecule to form DPE.

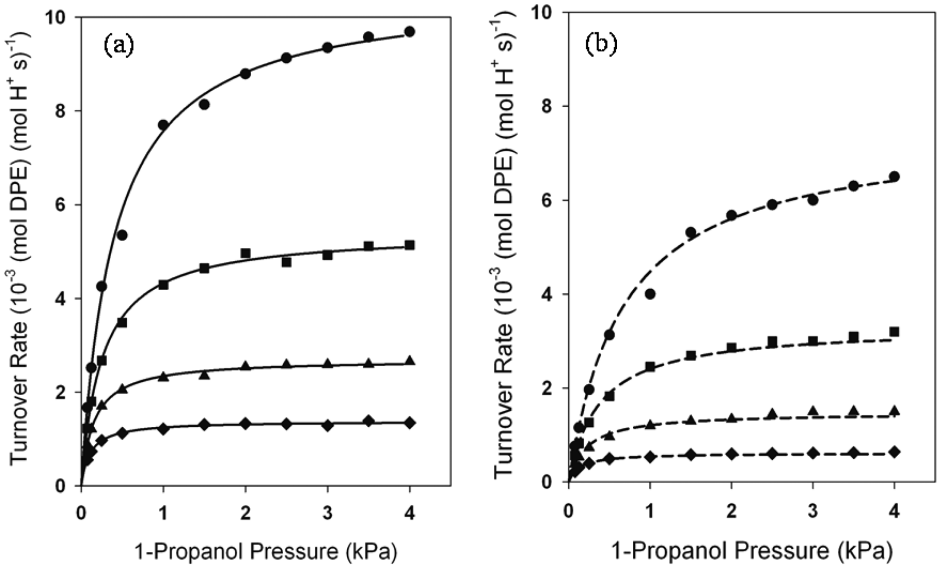

Figure 7. Measured DPE turnover rates (per H^{+}) as a function of 1-propanol pressure (0.075−4 kPa) over H-MFI-15-AHFS at 413 K (◆), 423 K (▲), 433 K (■), and 443 K (●). The solid and dash curves represent the fitting of experimental data points to eq 5: (a) in the absence of co-fed water; (b) in the presence of co-fed water (P_{water} = 0.53 kPa).

DOI: 10.1021/jacs.5b09107
J. Am. Chem. Soc. 2015, 137, 15781−15794

Scheme 2. A Proposed Sequence of Elementary Steps for 1-Propanol Dehydration to Form DPE over a Zeolitic Proton

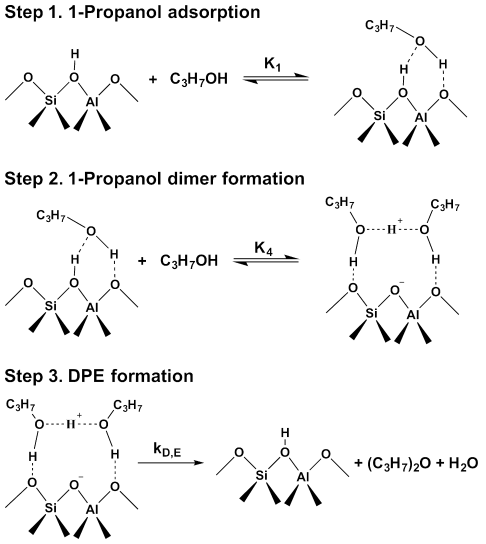

The sequential mechanism shares the same rate-limiting step with the E1-like mechanism for 1-propanol monomer to propene. Thus, the rate equation for water elimination from monomeric 1-propanol (eq 2) would be also applicable to the bimolecular 1-propanol dehydration to DPE via the sequential pathway. Significant dimer coverages reflected in the second term in the denominator of eq 2 would cause a negative rate dependence with 1-propanol pressure. However, the measured turnover rates did not decrease with increasing 1-propanol pressure, indicating that the sequential mechanism is not involved in DPE formation.

The rate equation for the direct route of DPE formation (Scheme 2) is expressed as (derivations in Supporting Information):

$$\frac{r_{C_3H_7OC_3H_7}}{[H^+]_0} = \frac{k_{D,E}K_4[C_3H_7OH]}{1 + K_4[C_3H_7OH]} \quad (5)$$

in which $k_{D,E}$ is the rate constant for DPE formation (Step 3, Scheme 2) and K_4 is the adsorption equilibrium constant for protonated dimers (Step 2, Scheme 2), respectively. Eq 5 can be rewritten into a linear form, eq 6, which accurately describes the kinetic effects of 1-propanol pressure on DPE formation turnover rate as shown by the linear dependence of inverse DPE turnover rate on 1-propanol pressure (Figure 9S):

$$\frac{[H^+]_0}{r_{C_3H_7OC_3H_7}} = \frac{1}{k_{D,E}} + \frac{1}{k_{D,E}K_4[C_3H_7OH]} \quad (6)$$

The regression analysis of the pressure dependence of DPE formation turnover rates allows to derive individual values for intrinsic rate constant for dimer ($k_{D,E}$, Step 3, Scheme 2) and the equilibrium constant for 1-propanol dimer formation (K_4, Step 2, Scheme 2). These two parameters can be obtained from the values of the slopes and the intercepts in Figure 9S and are listed in Tables 5 and 6. The regressed rate constant for activation of 1-propanol dimer ($k_{D,E}$) increases from 1.4×10^{-3} to 10.5×10^{-3} $(H^+ s)^{-1}$ with increasing temperature from 413 to 443 K, concomitant with the decrease of equilibrium constant (K_4) from 9.1 to 2.5 kPa^{-1} in the absence of water.

In the presence of water, $k_{D,E}$ decreases by 53% and 39% at 413 and 443 K, respectively, indicating a more significant inhibiting effect at low temperatures. A reasonable agreement is found between the values of the equilibrium constant for the formation of the 1-propanol dimer (K_4 in Tables 2–6), evaluated from two independent sets of data, i.e., the 1-propanol pressure dependences of propene synthesis rates fitted with eq 4 and of DPE synthesis rates fitted with eq 6. This consistency, in the absence and presence of co-fed water, supports the reliability of the rate equations and mechanisms for propene and DPE synthesis proposed in Schemes 1 and 2, respectively.

Table 5. DPE Formation Rate $k_{D,E}$ and 1-Propanol Dimer Formation Equilibrium Constant K_4 (see Scheme 2) for Bimolecular 1-Propanol Dehydration to DPE over H-MFI-15-AHFS in the Absence of Co-Fed Water[a]

T (K)	$k_{D,E}$ 10^{-3} $(H^+ s)^{-1}$	K_4 (kPa^{-1})
413	1.4	9.1
423	2.7	6.5
433	5.4	4.0
443	10.5	2.5

[a]Parameters are determined by linear regression of experimental data to eq 6.

Table 6. DPE Formation Rate $k_{D,E}$ and 1-Propanol Dimer Formation Equilibrium Constant K_4 (see Scheme 2) for Bimolecular 1-Propanol Dehydration to DPE over H-MFI-15-AHFS in the Presence of Co-Fed Water (0.53–2.5 kPa)[a]

T (K)	$k_{D,E}$ 10^{-3} $(H^+ s)^{-1}$	K_4 (kPa^{-1})
413	0.7	17.3
423	1.6	10.0
433	3.3	6.5
443	6.4	3.8

[a]Parameters are determined by linear regression of experimental data to eq 6.

The activation enthalpies and entropies as well as the thermodynamic quantities for 1-propanol dimer formation (from monomer) were determined by plotting the rate and equilibrium constants against the reciprocal temperature, in the absence and presence of co-fed water (Figure 10S). As shown in Table 7, the activation enthalpy $\Delta H^{\ddagger}_{D,E}$ increases from 103 to 115 kJ mol^{-1} in the presence of water, demonstrating that water inhibits not only the unimolecular alcohol dehydration but also the bimolecular dehydration to ether. The activation entropy for DPE was negative ($\Delta S^{\ddagger}_{D,E} = -54$ J mol^{-1} K^{-1}), in agreement

Table 7. Activation Enthalpies, Entropies, and Free Energies for Bimolecular 1-Propanol Dehydration to DPE and Adsorption Enthalpies and Entropies for 1-Propanol Dimer Formation in the Absence and Presence of Co-Fed Water (0.53–2.5 kPa) over H-MFI-15-AHFS at 433 K[a]

	without water	with water
$\Delta H^{\ddagger}$ (kJ mol^{-1})	103 ± 1	115 ± 2
$\Delta S^{\ddagger}$ (J mol^{-1} K^{-1})	−54 ± 2	−30 ± 1
$\Delta G^{\ddagger}$ (kJ mol^{-1})	126 ± 2	128 ± 2
ΔH^{o}_{4} (kJ mol^{-1})	−66 ± 4	−76 ± 2
ΔS^{o}_{4} (J mol^{-1} K^{-1})	−103 ± 9	−122 ± 6

[a]For calculations of activation entropies from measured rate/equilibrium constants on the basis of transition-state theory, the standard states are defined as follows: P^o = 100 kPa for gaseous molecules and θ = 1 for surface species.

DOI: 10.1021/jacs.5b09107
J. Am. Chem. Soc. 2015, 137, 15781–15794

with the negative activation entropy reported for methanol dehydration to DME,[22] but in contrast to the positive activation entropy for propene formation ($\Delta S^{\ddagger}_{M,P}$ = 25 J mol^{-1} K^{-1}, $\Delta S^{\ddagger}_{D,P}$ = 91 J mol^{-1} K^{-1}). In the presence of intrazeolite water, the activation entropy for DPE formation ($\Delta S^{\ddagger}_{D,E}$) increases from −54 to −30 J mol^{-1} K^{-1}, concomitant with an increase in activation enthalpy. It is the increase in enthalpy (from 103 to 115 kJ mol^{-1}), rather than the concomitant entropy change, that makes the DPE formation unfavorable in the presence of water (increase of Gibbs free energy from 126 to 128 kJ mol^{-1}). The enthalpies and entropies for dimer formation (ΔH_4 and ΔS_4) evaluated from DPE formation kinetics are close to those evaluated from propene formation kinetics (Table 4).

Toward Understanding of the Impact of Water. The turnover rates for water elimination from 1-propanol to form propene (Figure 3) and the intermolecular dehydration to form DPE (Figure 7) decreased when water was co-fed. Similar observations have been reported for methanol, ethanol, and 2-butanol over zeolites, Al_2O_3, and heteropolyacids, where the presence of water decreased the rate of acid-catalyzed dehydration.[21,35,53,64]

Several potential causes for the negative impact of water on the Brønsted acid-catalyzed dehydration of alcohols over zeolites may exist. First, water may reduce the structural stability of zeolites at elevated temperatures. Acidic zeolites may suffer from the steam-induced cleavage of framework Al−O bonds, which leads to dealumination at elevated temperatures (>523 K);[65] the dehydration of simple alcohols were, however, studied typically between 343 and 433 K. The unchanged concentrations of BAS and LAS in the used catalyst, the fully restorable activity after removing water vapor, and the long-term stability (not shown) in the presence of water demonstrate that the H-MFI zeolite used in this work was highly stable under the reaction conditions explored (413−443 K, 0−2.5 kPa H_2O). These observations lead us to conclude that it is highly unlikely that hydrolysis of acid sites is responsible for the adverse effect of water.

The second cause could be competitive adsorption of water in the pores, leading to lower intrazeolite concentrations of 1-propanol and consequently lower concentrations of adsorbed reactive intermediates on the Brønsted-acidic active sites. To test this hypothesis, the co-adsorption of 1-propanol and water was studied in two distinct sequences over H-MFI-15-AHFS. In Mode A, water adsorption (5 × 10^{-4} kPa) was followed by 1-propanol adsorption (5 × 10^{-4} kPa); in Mode B, 1-propanol adsorption (5 × 10^{-4} kPa) was followed by water adsorption (5 × 10^{-4} kPa). The IR spectra are shown in Figure 8. The bands at 3745 and 3610 cm^{-1} of the activated HZSM-5 are assigned to terminal Si−OH groups and Brønsted-acidic Si−OH−Al groups, respectively (see also Figure 1).

When water was adsorbed first, the coverage remained low. The subsequent introduction of 1-propanol removed most of adsorbed water from the OH groups, demonstrating that 1-propanol interacts much more strongly with BAS than water. With the reverse sequence, first adsorbing 1-propanol and then water, adsorbed 1-propanol remained unchanged on BAS after the water was introduced. Thus, we conclude that 1-propanol is able to displace effectively adsorbed water, while water is hardly able to do so to adsorbed 1-propanol. This is also in line with the higher heat of adsorption of 1-propanol (−120 kJ mol^{-1}, as we show later) than of water (∼−55 kJ mol^{-1}, not shown). Thus, we conclude that water is very ineffective in competing with 1-propanol for the active site and is, therefore, unlikely to be able to influence significantly the intrazeolite concentration of adsorbed 1-propanol.

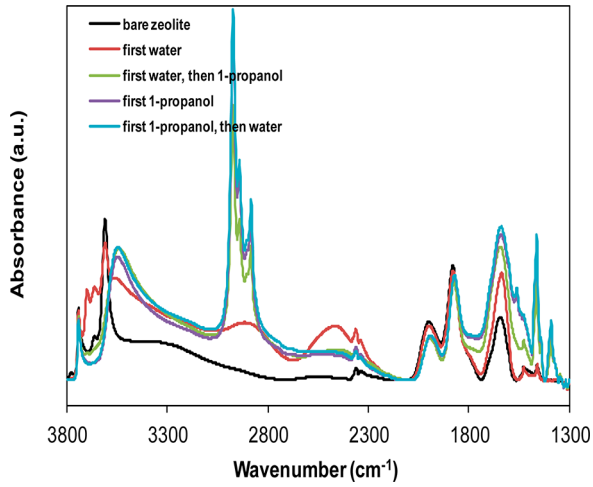

Figure 8. IR spectra for 1-propanol (5 × 10^{-4} kPa) and water (5 × 10^{-4} kPa) co-adsorption over H-MFI-15-AHFS at 323 K in two modes: water adsorption followed by 1-propanol adsorption or 1-propanol adsorption followed by water adsorption. All spectra were recorded at the indicated equilibrium partial pressures.

To arrive at a complete quantitative description of the energy landscape for this reaction, we derive next the adsorption enthalpies for the 1-propanol monomer and dimer intermediates interacting with BAS. The ratio of 1-propanol dimer and monomer coverage (θ_D/θ_M) can be derived from the formulas S-1 and S-2 (see S.1 in Supporting Information) to be K_4P (i.e., the product of dimer formation constant and 1-propanol pressure). From the adsorption enthalpies (ΔH_4) and entropies (ΔS_4) for 1-propanol dimer formation at 433 K (compiled in Tables 4 and 7), the equilibrium constant K_4 was estimated to be 1.4 × 10^3 (kPa)$^{-1}$ by extrapolating the adsorption temperature to 323 K, assuming ΔH_4 and ΔS_4 to be invariant with temperature. Consequently, θ_D/θ_M was determined to be ∼0.1 at 1-propanol partial pressure of 10^{-4} kPa corresponding to the first uptake point (coverage 0.025) in Figure 2, which suggests that the 1-propanol monomer is the dominant surface intermediate with the adsorption enthalpy of ∼−120−−130 kJ mol^{-1}. The value of θ_D/θ_M progressively increased to 1 and 6 at 1-propanol partial pressures of 6.0 × 10^{-4} and 4.2 × 10^{-3} kPa (corresponding to the third and sixth uptake points in Figure 2), respectively. This points to a crucial fact that the 1-propanol dimer is present as the dominant adsorbed species even when a majority of the BAS are still uncovered (at 323 K). The integral heats for the 1-propanol dimer formation (from two 1-propanol molecules) can be estimated to be ∼−184 kJ mol^{-1} from calorimetry data. In turn, the difference in the measured adsorption enthalpies for the monomer and the dimer would be ∼−64 kJ mol^{-1}, in remarkable agreement with the value derived from kinetic measurements (−64−−66 kJ mol^{-1}; Tables 4 and 7). Note that an overall higher heat was reported for 1-propanol adsorption on HZSM-5 in earlier contributions,[51] where calorimetry data were taken at temperatures (e.g., 400 K) at which exothermic ether formation would occur.

Figure 9 illustrates the energy diagram for 1-propanol monomer and the dimer dehydration to form propene in the absence and presence of water. The heat of adsorption of −120 kJ mol^{-1} for 1-propanol monomer formation was adopted as

DOI: 10.1021/jacs.5b09107
J. Am. Chem. Soc. 2015, 137, 15781−15794

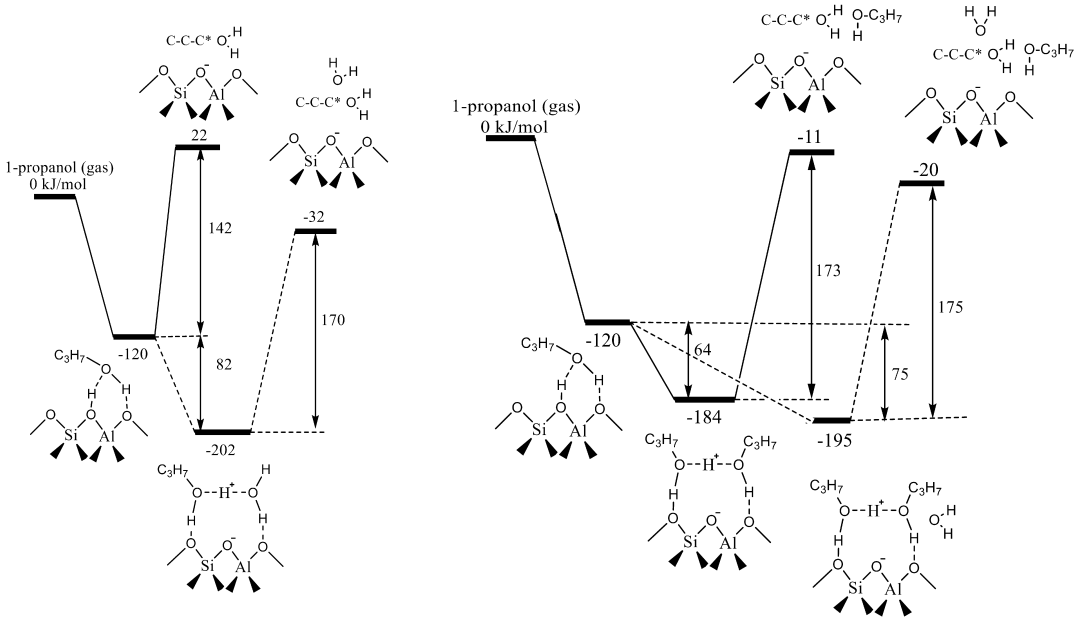

Figure 9. Illustrative energy diagrams for 1-propanol monomer- (left) and dimer-mediated (right) dehydration to propene, in the absence (solid line) and presence of intrazeolite water (dashed line). All denoted values, except for the enthalpy associated with the formation of the 1-propanol-water dimer, are from experiments (i.e., calorimetric and kinetic measurements).

discussed above. The transition-state energy of 22 kJ mol^{-1} is directly derived from the experimentally measured activation enthalpy of 142 kJ mol^{-1}. When water is present in the pores, it can interact with adsorbed monomeric 1-propanol. One possibility is to form a protonated 1-propanol-water dimer, and the enthalpy for this mixed dimer formation is −82 kJ mol^{-1} (DFT-calculations, see Figure 11S).

On the basis of the calculated 1-propanol and water dimer formation enthalpy of −82 kJ mol^{-1} and the measured activation enthalpy of 170 kJ mol^{-1}, the enthalpy of the elimination transition state is determined to be −32 kJ mol^{-1}, which indicates that water stabilizes the transition state by 52 kJ mol^{-1} relative to the transition-state enthalpy of 22 kJ mol^{-1} without additional water introduced. Hence, it seems that water stabilizes the adsorption intermediate (82 kJ mol^{-1} more stabilized) to a greater extent than the transition state (52 kJ mol^{-1} more stabilized), resulting in the higher activation barrier for propene formation. A similar observation was made in 2-butanol dehydration over POM clusters;[34] however, in that work, the mixed 2-butanol-water dimer must be unreactive in order to explain the kinetic data. It is important to add that one is advised against making quantitative comparisons between the energies of the 1-propanol-water complex and the 1-propanol dimer (−202 vs −184 kJ mol^{-1} as denoted in Figure 9), as a result of the different uncertainties inherent in the used approaches to obtain these values (i.e., DFT and experiments/kinetic simulation). It is only safe to conclude that the two species have comparable enthalpic stabilities.

DFT calculations were employed to investigate the effects of additional 1-propanol and water molecules on the energetics landscape and to provide structural descriptions of the relevant intermediate and transition states (Figures 12S and 13S). These theoretical evaluations confirmed the presence of dimeric species and the experimentally observed trend that a water molecule or a second 1-propanol molecule in the vicinity of the adsorbed monomer stabilizes that monomer species to a greater extent than the transition state, resulting in increased activation barriers. The agreement is remarkably good between the experimentally determined energy landscape (Figure 9) and the theoretically assessed one (Figure 12S).

Despite the concurrent increase in activation entropy from 25 to 87 J mol^{-1} K^{-1} (Table 4), the higher standard Gibbs free energy (relatively low reaction temperature) leads to an inhibition by water. This demonstrates that the strong stabilization of the adsorbed intermediates before the rate-determining step is the primary factor in determining the high activation barrier and in turn causing the lower dehydration rate.

This action of water is analogous to the role that a second 1-propanol molecule plays in reducing the rate in comparison to the water elimination from a monomeric 1-propanol. Subsequent to adsorption of a single 1-propanol (ΔH_{ads} = −120 kJ mol^{-1}), the adsorption of a second 1-propanol molecule forms the dimer with a lower enthalpy (ΔH_{ads} = −64 kJ mol^{-1}). Because the measured activation enthalpy was 173 kJ mol^{-1}, the transition-state energy was determined to be −11 kJ mol^{-1}, which is comparable to the transition-state energy of −32 kJ mol^{-1} for 1-propanol monomer to propene in the presence of water. Thus, we conclude that a water molecule and an additional molecule of 1-propanol stabilize the adsorbed as well as the transition state to the same extent, affecting the rates in an almost identical fashion.

The energy diagram of DPE formation (Figure 10) shows that the transition-state energy of −81 kJ mol^{-1} is significantly lower than that for propene formation (22 kJ mol^{-1} for the 1-propanol monomer to propene and −11 kJ mol^{-1} for the 1-propanol dimer to propene), implying the more effective stabilization of the carbenium ion by 1-propanol (DPE formation) than by water on the propyl cation in transition state (propene formation). The introduced water stabilizes the adsorbed intermediate (11 kJ mol^{-1} more stable), but the transition-state energy is hardly influenced.

DOI: 10.1021/jacs.5b09107
J. Am. Chem. Soc. 2015, 137, 15781−15794

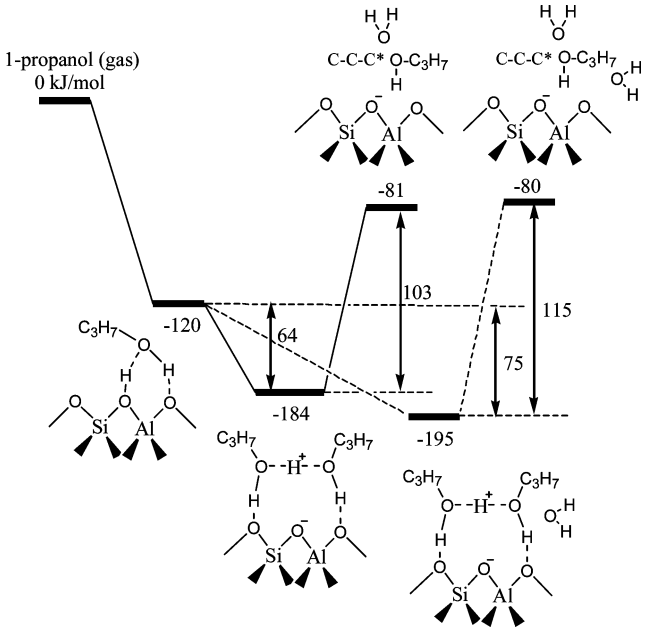

Figure 10. An illustrative energy diagram for 1-propanol bimolecular dehydration to form DPE in the absence (solid line) and presence of water (dashed line). The denoted values are directly measured or derived from experiments (i.e., calorimetric and kinetic measurements).

CONCLUSION

1-Propanol dehydration to propene and DPE was explored, in the absence and presence of co-fed water, to derive an explicit model of the elementary steps with the corresponding energetics. It is shown that monomeric and dimeric species from 1-propanol are both able to eliminate water, forming propene. The dimeric species becomes dominant at moderate to high 1-propanol pressures. A Langmuir model was developed for both cases, and the kinetic equations describe the two reaction pathways across the whole temperature and pressure range studied. 1-Propanol bimolecular dehydration to DPE proceeds via a direct/associative route.

Water retards the rate to propene and DPE. Neither the destruction of acid sites by water nor the competitive adsorption of water accounts for the observed decrease in reaction rates in the presence of co-fed water. The catalysts have been shown to be extremely structurally stable under reaction conditions. In addition, *in situ* IR spectroscopy demonstrates that 1-propanol adsorption on BAS can hardly be impeded by water having a much weaker heat of adsorption.

The quantitative analysis of the kinetics shows that the inhibiting impact of water is related to the different stabilization of the adsorbed intermediate prior to the transition state. Water stabilizes the adsorbed 1-propanol intermediate better than the transition state enthalpically, which causes a higher activation barrier for the elimination step. Additional 1-propanol involved in 1-propanol dimer to propene route inhibits the dehydration rate in a manner consistent with the introduced water. An additional 1-propanol molecule stabilizes the adsorbed intermediate and the transition state enthalpically to the same extent as water, inhibiting dehydration similarly.

These findings explain unequivocally the role of water and similar polar molecules in changing the rate of reactions by stabilizing the ground state of the reactant much more effectively than the transition state. It eliminates a number of speculations on the role of stability of acid sites (or changes in their acid strength) as well as of the role of competitive adsorption and by doing so helps in devising rational strategies to subtly adjust reaction pathways.

EXPERIMENTAL AND THEORY SECTION

Zeolite Samples and AHFS Treatment. The NH_4-ZSM-5 sample was provided by Zeolyst International (CBV3024E, Si/Al = 15). To minimize the effect of extra-framework Al on the acidity or local environment of acid sites, this NH_4-ZSM-5 sample was treated with AHFS to remove the extra-framework Al. The procedure is as follows: 2 g NH_4-ZSM-5 sample was added into 80 mL deionized water stirred in a 100 mL PTFE-liner, followed by the addition of 1.42 g (8.0 mmol) AHFS to the solution and then stirred vigorously at 353 K for 5 h. The resulting products were centrifuged, rinsed six times with hot deionized water (353 K), and then dried overnight at 393 K. The proton-form of both parent and AHFS-treated HZSM-5 was obtained by calcinations at 823 K for 5 h in 100 mL min^{-1} synthetic air with a heating rate of 10 K min^{-1}.

Zeolite Characterization Methods. Specific surface area and porosity were analyzed by N_2 adsorption−desorption isotherms recorded on an automated BET system (PMI automated Sorptomatic 1990) at liquid nitrogen temperature (77 K). The samples were outgassed in vacuum ($p = 10^{-4}$ kPa) at 523 K for 2 h prior to adsorption.

Elemental analysis of the samples was determined by atomic absorption spectroscopy (AAS) using a Unicam M Series Flame-AAS equipped with an FS 95 autosampler and a GF 95 graphite furnace.

The *in situ* infrared (IR) spectra of adsorbed 1-propanol were recorded on a Bruker Vertex 70 spectrometer (resolution 4 cm^{-1}) in the transmission absorption mode. The samples were pressed into self-supporting wafers and activated in vacuum ($p < 10^{-7}$ kPa) at 723 K for 1 h. The equilibration between the zeolite and the gas-phase molecules was monitored in a time-resolved manner. All spectra were first baseline-corrected in the range of 3800−1300 cm^{-1} and then normalized by the integral peak area of the overtones of framework vibration band between 2100 and 1735 cm^{-1}.

The concentration of acid sites was measured by IR spectroscopy of adsorbed pyridine recorded on a Thermo Nicolet 5700 FTIR apparatus with a resolution of 2 cm^{-1}. The self-supporting wafer was activated in vacuum for 1 h at 723 K at a heating rate of 10 K min^{-1}. After cooling to 423 K, pyridine (10^{-2} kPa) was admitted to the cell and then adsorbed for 1 h. Subsequently, spectra were collected after outgassing for 0.5 h at 423 K. The bands located at 1540 and 1450 cm^{-1} are assigned to BAS and LAS, respectively. For quantification, the molar integral extinction coefficients of 0.73 and 0.96 cm μmol^{-1} were used for BAS and LAS, respectively.[66]

Gravimetric and Calorimetric Measurements. The measurements were carried out with a Setaram TG-DSC 111 thermoanalyzer with a Baratron pressure transducer. The samples were pressed into thin wafers and subsequently broken into small platelets. Then 10−15 mg of the platelets were charged into a quartz sample holder of the balance and activated at 723 K for 1 h with a heating ramp of 10 K min^{-1} under vacuum ($p < 10^{-7}$ kPa). After cooling down to 323 K, 1-propanol vapor was stepwise introduced into the closed system and equilibrated in the pressure range from 10^{-4} to 1.2 kPa. The weight increase and heat flux were monitored during pressure equilibration. The heats of adsorption were directly obtained by integration of the recorded heat flux signal observed during stepwise increase of 1-propanol pressure. The surface coverage is calculated via normalizing the uptake of adsorption by the concentration of BAS determined from pyridine-IR measurement.

Catalytic Measurements of 1-Propanol Dehydration. The steady-state catalytic dehydration reactions of 1-propanol (Sigma-Aldrich, >99% GC assay) were carried out in a continuous quartz tubular flow reactor with an inner diameter of 4 mm under atmospheric pressure. AHFS-treated MFI samples were pressed and sieved to retain 160−280 μm aggregates, and the mass of catalyst (2−230 mg) used for catalytic measurements was adjusted to maintain

DOI: 10.1021/jacs.5b09107
J. Am. Chem. Soc. 2015, 137, 15781−15794

differential conversion below 1.5%. Preliminary tests confirmed that diffusion of molecules to and from the active centers is not rate limiting, that all the Brønsted acid OH groups are accessible to reagent molecules, and that secondary reactions such as propene oligomerization are negligible under the applied conditions. The catalyst was then diluted with acid-washed SiO_2 to maintain the total sample mass no less than 0.1 g in all experiments. A K-type thermocouple was used to measure the bed temperature, which was retained at reaction temperature (413−443 K) using a resistively heated tube furnace. The sample was heated to 773 K with a ramp rate of 10 K min^{-1} in He flow (40 mL min^{-1}), kept for 1 h, and then cooled to reaction temperatures before catalytic measurements. All the transfer lines were held at 383 K to prevent condensation of reactants and products.

Saturated 1-propanol vapor was introduced into the reactor by He carrier gas via a saturator (thermostated in a variable-temperature water bath). When studying the effect of water, the saturated water vapor was separately fed into the reactor by an additional stream of He passing through another thermostated saturator containing pure liquid water, while adjusting the bath temperature for the 1-propanol saturator so that the partial pressure of 1-propanol and its space time were not changed. Taking 1-propanol partial pressure of 2.5 kPa as an example, the saturator temperature was maintained at 296.5 K, and the He gas flow rate was set to 40 mL min^{-1} in the absence of co-fed water. When introducing water, the 1-propanol saturator temperature was correspondingly adjusted to 307.6 K to achieve a 1-propanol vapor pressure of 5 kPa, and the 1-propanol-carrying He flow rate was reduced to 20 mL min^{-1}; meanwhile, another stream of He with a flow rate of 20 mL min^{-1} passed through the saturator containing water kept at 281.1 K (water partial pressure of 1.06 kPa) to achieve the 1-propanol and water partial pressures of 2.5 and 0.53 kPa, respectively. The concentrations of reactants and products were analyzed by a gas chromatography (GC) Hewlett-Packard 5890 (Series II) equipped with a flame ionization detector (FID) and a Supelco-Wax column. No products were detected during blank tests in empty reactors or in reactors filled only with SiO_2 diluent. Kinetic data were measured at conversion levels below 1.5% (typically below1%; representative plots of rates as a function of conversion and space velocity are shown in Figure 2S), while the stability measurement was performed at the highest reaction temperature of 443 K. Deactivation was not observed on the sample used for this study. The SigmaPlot software was used to estimate the kinetic parameters.

Computational Methods. Periodic DFT calculations were carried out using the CP2K code.[67] All calculations employed a mixed Gaussian and plane wave basis sets. Core electrons were represented with norm-conserving Goedecker−Teter−Hutter pseudopotentials,[68−70] and the valence electron wave function was expanded in a double-ζ basis set with polarization functions[71] along with an auxiliary plane wave basis set with an energy cutoff of 360 eV. The generalized gradient approximation exchange−correlation functional of Perdew, Burke, and Enzerhof (PBE)[72] was used. Test calculations showed that the total energy change of the reactive system was negligible (<0.01 eV) when the maximum force convergence criteria of 0.001 hartree/bohr was used. Each reaction-state configuration was optimized with the Broyden−Fletcher−Goldfarb−Shanno (BGFS) algorithm with SCF convergence criteria of 1.0×10^{-8} au. Previous experimental measurements[51] and DFT calculations[61] of primary alcohols adsorption in HZSM-5 zeolite indicated that the dispersive vdW interactions between the adsorbed alcohols and the BAS in the zeolite significantly stabilize the adsorbed molecule by adding adsorption enthalpy of 10−15 kJ mol^{-1} for each carbon atom. To compensate the long-range dispersion interaction between the adsorbate and the zeolite, the DFT-D3 scheme[73] with an empirical damped potential term was added into the energies obtained from exchange−correlation functional in all calculations. Transition states of elementary steps in the dehydration and etherification reaction routes were located using the CI-NEB method[74,75] with seven intermediate images along the reaction pathway between initial and final states. The identified transition states were confirmed by vibrational analysis. Only one imaginary frequency was found for each transition state.

For the acid-catalyzed reaction catalyzed over zeolites, the confinement and steric hindrance strongly affect the stabilities of reaction intermediates and transition states. To account for important entropic contribution and ZPE corrections, both Gibbs free energy (ΔG) and enthalpy (ΔH) changes along reaction pathways were calculated (see Supporting Information).[76]

A periodic three-dimensional HZSM-5 zeolite structure of $Si_{96}O_{192}$ with experimental lattice parameters of 20.022 × 19.899 × 13.383 $Å^3$ was used in this work. The unit cell of the HZSM-5 with Si/Al = 23 then was built by replacing four Si atoms at T sites of T4, T9, T10, T12 with four Al atoms. The resulting negative charges were compensated by adding four H atoms at the oxygen atoms which are close neighbors of Al atoms on the zeolite frame, yielding the active Brønsted acidic sites, i.e., Si−O(H)−Al of the HZSM-5 shown in Figure 14S. The T12 site was used as the active acid site for dehydration throughout the calculations.

■ ASSOCIATED CONTENT

Supporting Information

The Supporting Information is available free of charge on the ACS Publications website at DOI: 10.1021/jacs.5b09107.

The derivations of kinetic equations based on the proposed mechanistic sequences, additional figures and coordinates of optimized structures (PDF)

■ AUTHOR INFORMATION

Corresponding Author

*Johannes.Lercher@ch.tum.de, johannes.lercher@pnnl.gov

Notes

The authors declare no competing financial interest.

■ ACKNOWLEDGMENTS

This work was supported by the U.S. Department of Energy (DOE), Office of Basic Energy Sciences, Division of Chemical Sciences, Geosciences & Biosciences. Portions of the computational work were performed using resources at EMSL (a DOE Office of Science User Facility sponsored by the Office of Biological and Environmental Research and located at Pacific Northwest National Laboratory) and NERSC (the National Energy Research Scientific Computing Center, a DOE Office of Science User Facility supported by the Office of Science of the U.S. Department of Energy under Contract No. DE-AC02-05CH11231). PNNL is a multiprogram national laboratory operated for DOE by Battelle Memorial Institute under contract no. DE-AC05-76RL01830.

■ REFERENCES

(1) Moser, W. R.; Thompson, R. W.; Chiang, C. C.; Tong, H. *J. Catal.* **1989**, *117*, 19−32.

(2) Gayubo, A. G.; Alonso, A.; Valle, B.; Aguayo, A. T.; Bilbao, J. *Appl. Catal., B* **2010**, *97*, 299−306.

(3) Kim, Y. T.; Jung, K. D.; Park, E. D. *Appl. Catal., A* **2011**, *393*, 275−287.

(4) Kongpatpanich, K.; Nanok, T.; Boekfa, B.; Probst, M.; Limtrakul, J. *Phys. Chem. Chem. Phys.* **2011**, *13*, 6462−6470.

(5) Kim, Y. T.; Jung, K. D.; Park, E. D. *Microporous Mesoporous Mater.* **2010**, *131*, 28−36.

(6) Zhao, C.; Camaioni, D. M.; Lercher, J. A. *J. Catal.* **2012**, *288*, 92−103.

(7) Roy, S.; Mpourmpakis, G.; Hong, D. Y.; Vlachos, D. G.; Bhan, A.; Gorte, R. J. *ACS Catal.* **2012**, *2*, 1846−1853.

(8) Kostestkyy, P.; Yu, J.; Gorte, R. J.; Mpourmpakis, G. *Catal. Sci. Technol.* **2014**, *4*, 3861−3869.

(9) Young, L. B.; Butter, S. A.; Kaeding, W. W. *J. Catal.* **1982**, *76*, 418−432.

DOI: 10.1021/jacs.5b09107
J. Am. Chem. Soc. 2015, 137, 15781−15794

(10) Mirth, G.; Ĉejka, J.; Lercher, J. A. *J. Catal.* **1993**, *139*, 24−33.
(11) Chen, N. Y. *J. Catal.* **1979**, *59*, 123−129.
(12) Stöcker, M. *Microporous Mesoporous Mater.* **1999**, *29*, 3−48.
(13) Svelle, S.; Joensen, F.; Nerlov, J.; Olsbye, U.; Lillerud, K. P.; Kolboe, S.; Bjorgen, M. *J. Am. Chem. Soc.* **2006**, *128*, 14770−14771.
(14) Choi, M.; Na, K.; Kim, J.; Sakamoto, Y.; Terasaki, O.; Ryoo, R. *Nature* **2009**, *461*, 246−249.
(15) Ilias, S.; Bhan, A. *ACS Catal.* **2013**, *3*, 18−31.
(16) Sun, X. Y.; Müller, S.; Shi, H.; Haller, G. L.; Sanchez-Sanchez, M.; van Veen, A. C.; Lercher, J. A. *J. Catal.* **2014**, *314*, 21−31.
(17) Fraenkel, D.; Cherniavsky, M.; Ittah, B.; Levy, M. *J. Catal.* **1986**, *101*, 273−283.
(18) Wu, P.; Komatsu, T.; Yashima, T. *Microporous Mesoporous Mater.* **1998**, *22*, 343−356.
(19) Ahn, J. H.; Kolvenbach, R.; Al-Khattaf, S. S.; Jentys, A.; Lercher, J. A. *ACS Catal.* **2013**, *3*, 817−825.
(20) Makarova, M. A.; Paukshtis, E. A.; Thomas, J. M.; Williams, C.; Zamaraev, K. I. *J. Catal.* **1994**, *149*, 36−51.
(21) Chiang, H.; Bhan, A. *J. Catal.* **2010**, *271*, 251−261.
(22) Jones, A. J.; Iglesia, E. *Angew. Chem., Int. Ed.* **2014**, *53*, 12177−12181.
(23) Williams, C.; Makarova, M. A.; Malysheva, L. V.; Paukshtis, E. A.; Zamaraev, K. I.; Thomas, J. M. *J. Chem. Soc., Faraday Trans.* **1990**, *86*, 3473−3485.
(24) Stepanov, A. G.; Zamaraev, K. I.; Thomas, J. M. *Catal. Lett.* **1992**, *13*, 407−422.
(25) Makarova, M. A.; Williams, C.; Romannikov, V. N.; Zamaraev, K. I.; Thomas, J. M. *J. Chem. Soc., Faraday Trans.* **1990**, *86*, 581−584.
(26) Jia, C. J.; Liu, Y.; Schmidt, W.; Lu, A. H.; Schüth, F. *J. Catal.* **2010**, *269*, 71−79.
(27) Corma, A.; Huber, G. W.; Sauvanaud, L.; O'Connor, P. *J. Catal.* **2008**, *257*, 163−171.
(28) Jones, A. J.; Carr, R. T.; Zones, S. I.; Iglesia, E. *J. Catal.* **2014**, *312*, 58−68.
(29) Kofke, T. J. G.; Gorte, R. J.; Farneth, W. E. *J. Catal.* **1988**, *114*, 34−45.
(30) Aronson, M. T.; Gorte, R. J.; Farneth, W. E. *J. Catal.* **1986**, *98*, 434−443.
(31) Aronson, M. T.; Gorte, R. J.; Farneth, W. E. *J. Catal.* **1987**, *105*, 455−468.
(32) Kondo, J. N.; Nishioka, D.; Yamazaki, H.; Kubota, J.; Domen, K.; Tatsumi, T. *J. Phys. Chem. C* **2010**, *114*, 20107−20113.
(33) Kondo, J. N.; Yamazaki, H.; Osuga, R.; Yokoi, T.; Tatsumi, T. *J. Phys. Chem. Lett.* **2015**, *6*, 2243−2246.
(34) Macht, J.; Janik, M. J.; Neurock, M.; Iglesia, E. *J. Am. Chem. Soc.* **2008**, *130*, 10369−10379.
(35) Dewilde, J. F.; Chiang, H.; Hickman, D. A.; Ho, C. R.; Bhan, A. *ACS Catal.* **2013**, *3*, 798−807.
(36) Ison, A.; Gorte, R. J. *J. Catal.* **1984**, *89*, 150−158.
(37) Rice, M. J.; Chakraborty, A. K.; Bell, A. T. *J. Phys. Chem. A* **1998**, *102*, 7498−7504.
(38) Jungsuttiwong, S.; Limtrakul, J.; Truong, T. N. *J. Phys. Chem. B* **2005**, *109*, 13342−13351.
(39) Jentys, A.; Warecka, G.; Derewinski, M.; Lercher, J. A. *J. Phys. Chem.* **1989**, *93*, 4837−4843.
(40) Kondo, J. N.; Iizuka, M.; Domen, K.; Wakabayashi, F. *Langmuir* **1997**, *13*, 747−750.
(41) Pelmenschikov, A. G.; Vansanten, R. A. *J. Phys. Chem.* **1993**, *97*, 10678−10680.
(42) Zygmunt, S. A.; Curtiss, L. A.; Iton, L. E.; Erhardt, M. K. *J. Phys. Chem.* **1996**, *100*, 6663−6671.
(43) Sauer, J.; Ugliengo, P.; Garrone, E.; Saunders, V. R. *Chem. Rev.* **1994**, *94*, 2095−2160.
(44) Krossner, M.; Sauer, J. *J. Phys. Chem.* **1996**, *100*, 6199−6211.
(45) Zheng, A. M.; Han, B.; Li, B. J.; Liu, S. B.; Deng, F. *Chem. Commun.* **2012**, *48*, 6936−6938.
(46) Janda, A.; Bell, A. T. *J. Am. Chem. Soc.* **2013**, *135*, 19193−19207.
(47) Jentys, A.; Warecka, G.; Lercher, J. A. *J. Mol. Catal.* **1989**, *51*, 309−327.
(48) Schallmoser, S.; Ikuno, T.; Wagenhofer, M. F.; Kolvenbach, R.; Haller, G. L.; Sanchez-Sanchez, M.; Lercher, J. A. *J. Catal.* **2014**, *316*, 93−102.
(49) Li, S. H.; Zheng, A. M.; Su, Y. C.; Zhang, H. L.; Chen, L.; Yang, J.; Ye, C. H.; Deng, F. *J. Am. Chem. Soc.* **2007**, *129*, 11161−11171.
(50) Thamm, H. *J. Chem. Soc., Faraday Trans. 1* **1989**, *85*, 1−9.
(51) Lee, C. C.; Gorte, R. J.; Farneth, W. E. *J. Phys. Chem. B* **1997**, *101*, 3811−3817.
(52) Lee, K. Y.; Arai, T.; Nakata, S.; Asaoka, S.; Okuhara, T.; Misono, M. *J. Am. Chem. Soc.* **1992**, *114*, 2836−2842.
(53) Macht, J.; Janik, M. J.; Neurock, M.; Iglesia, E. *Angew. Chem., Int. Ed.* **2007**, *46*, 7864−7868.
(54) Janik, M. J.; Macht, J.; Iglesia, E.; Neurock, M. *J. Phys. Chem. C* **2009**, *113*, 1872−1885.
(55) Alharbi, W.; Brown, E.; Kozhevnikova, E. F.; Kozhevnikov, I. V. *J. Catal.* **2014**, *319*, 174−181.
(56) Antal, M. J.; Carlsson, M.; Xu, X.; Anderson, D. G. M. *Ind. Eng. Chem. Res.* **1998**, *37*, 3820−3829.
(57) Kwak, J. H.; Rousseau, R.; Mei, D. H.; Peden, C. H. F.; Szanyi, J. *ChemCatChem* **2011**, *3*, 1557−1561.
(58) Wang, W.; Jiao, J.; Jiang, Y. J.; Ray, S. S.; Hunger, M. *ChemPhysChem* **2005**, *6*, 1467−1469.
(59) Blaszkowski, S. R.; vanSanten, R. A. *J. Am. Chem. Soc.* **1997**, *119*, 5020−5027.
(60) Nguyen, C. M.; Reyniers, M. F.; Marin, G. B. *Phys. Chem. Chem. Phys.* **2010**, *12*, 9481−9493.
(61) Nguyen, C. M.; Reyniers, M. F.; Marin, G. B. *J. Catal.* **2015**, *322*, 91−103.
(62) Xin, H. C.; Li, X. P.; Fang, Y.; Yi, X. F.; Hu, W. H.; Chu, Y. Y.; Zhang, F.; Zheng, A. M.; Zhang, H. P.; Li, X. B. *J. Catal.* **2014**, *312*, 204−215.
(63) Carr, R. T.; Neurock, M.; Iglesia, E. *J. Catal.* **2011**, *278*, 78−93.
(64) Santacesaria, E.; Gelosa, D.; Giorgi, E.; Carra, S. *J. Catal.* **1984**, *90*, 1−9.
(65) Gounder, R. *Catal. Sci. Technol.* **2014**, *4*, 2877−2886.
(66) Maier, S. M.; Jentys, A.; Lercher, J. A. *J. Phys. Chem. C* **2011**, *115*, 8005−8013.
(67) VandeVondele, J.; Krack, M.; Mohamed, F.; Parrinello, M.; Chassaing, T.; Hutter, J. *Comput. Phys. Commun.* **2005**, *167*, 103−128.
(68) Goedecker, S.; Teter, M.; Hutter, J. *Phys. Rev. B: Condens. Matter Mater. Phys.* **1996**, *54*, 1703−1710.
(69) Hartwigsen, C.; Goedecker, S.; Hutter, J. *Phys. Rev. B: Condens. Matter Mater. Phys.* **1998**, *58*, 3641−3662.
(70) Krack, M.; Parrinello, M. *Phys. Chem. Chem. Phys.* **2000**, *2*, 2105−2112.
(71) VandeVondele, J.; Hutter, J. *J. Chem. Phys.* **2007**, *127*, 114105.
(72) Perdew, J. P.; Burke, K.; Ernzerhof, M. *Phys. Rev. Lett.* **1996**, *77*, 3865−3868.
(73) Grimme, S.; Antony, J.; Ehrlich, S.; Krieg, H. *J. Chem. Phys.* **2010**, *132*, 154104−154119.
(74) Henkelman, G.; Uberuaga, B. P.; Jonsson, H. *J. Chem. Phys.* **2000**, *113*, 9901−9904.
(75) Mills, G.; Jonsson, H.; Schenter, G. K. *Surf. Sci.* **1995**, *324*, 305−337.
(76) John, M.; Alexopoulos, K.; Reyniers, M. F.; Marin, G. B. *J. Catal.* **2015**, *330*, 28−45.

DOI: 10.1021/jacs.5b09107
J. Am. Chem. Soc. 2015, 137, 15781−15794